Digital Signal Processing 135 (2023) 103942

Contents lists available at ScienceDirect

Digital Signal Processing

journal homepage: www.elsevier.com/locate/dsp

Moving target detection in range-ambiguous clutter scenario with PA-FDA dual-mode radar ☆

Zhixin Liu [a], Shengqi Zhu [a,*], Jingwei Xu [a], Xiongpeng He [a], Qi Liu [b,c]

[a] National Laboratory of Radar Signal Processing, Xidian University, Xi'an, China
[b] School of Future Technology, South China University of Technology, Guangzhou, China
[c] Pazhou Lab, Guangzhou, China

ARTICLE INFO

Article history:
Available online 31 January 2023

Keywords:
Frequency diverse array
Phased array
Airborne forward-looking array
Range-ambiguous clutter
Space-time adaptive processing

ABSTRACT

Range-ambiguous clutter suppression is challenging for airborne radar in non-sidelooking geometry. The target detection performance might degrade severely due to range ambiguity and range dependence problems. It is proved that the frequency diverse array (FDA) is capable of resolving the range ambiguity and is beneficial for range ambiguous clutter suppression. However, FDA uses wide coverage transmit beampattern, which causes somewhat gain loss compared to the phased array (PA). In this paper, we establish a PA-FDA dual-mode radar to maximize the advantages of PA and FDA radars to improve target detection performance in range-ambiguous clutter scenario. Firstly, the range ambiguous resolvability of FDA is utilized, where range ambiguous clutters are separated by using pre-filtering before space-time adaptive processing. Therefore, the range dependence compensation algorithms can be performed independently to further address the range dependence problem of non-sidelooking array radar. In this case, the clutter covariance matrix (CCM) is reconstructed by using linear combination of distinguishable CCMs corresponding to different range regions, resulting in improved accuracy of CCM estimation. Secondly, the enhanced CCM is applied in PA counterpart, which maximizes the high beampattern gain of PA and range ambiguity resolvability of FDA. It is verified that the PA-FDA dual-mode radar outperforms the PA or FDA single-mode in simultaneously narrow-beam detection and wide-angle coverage. Thus, the proposed PA-FDA dual-mode radar can greatly contribute to searching and tracking tasks. Simulation examples demonstrate the effectiveness of the proposed method.

1. Introduction

Airborne Early Warning has gained wide attention in the past decades, wherein the space-time adaptive processing (STAP) plays a pivotal role in target detection under the background of strong ground clutter and jamming [1][2][3]. With the increase in the maximum detectable range as well as the operational frequency, the contradiction between range and Doppler ambiguities becomes more and more serious. Generally, a medium or high pulse repetition frequency (PRF) is employed to alleviate the Doppler ambiguity. In the non-sidelooking array geometry of airborne radar, the range ambiguity and range dependence of clutter occur simultaneously, which causes severe performance degradation of clutter suppression as well as target detection [4][5]. The Range-dependence of clutter violates the basic assumption in STAP radar, i.e., the training samples are independent and identically distributed (IID) [6]. To handle this problem, several range dependence compensation algorithms have been developed, including derivative-based updating [7], Doppler warping (DW) [5], angular-Doppler compensation (ADC) [8], registration-based compensation [9], and space-time interpolation [10]. These algorithms are

☆ This work was supported in part by the Nature Science Foundation of China under Grants 61931016, 62071344, 61911530246, 62202174, and 62201408, in part by the Key Laboratory Equipment Advanced Research Fund under Grant 6142206200210, in part by the Science and Technology Innovation Team of Shaanxi Province under Grant 2022TD-38, in part by the Natural Science Basic Research Program of Shaanxi (No. 2023-JC-JQ-55), in part by the Innovation Capability Support Program of Shaanxi (No. 2022KJXX-38), in part by the stabilization support of National Radar Signal Processing Laboratory under Grant JKW202108, and in part by the Guangdong Provincial Key Laboratory of Human Digital Twin 2022B1212010004.

* Corresponding author.
E-mail addresses: liuzhixin_cauc@163.com (Z. Liu), zhushengqi8@163.com (S. Zhu), xujingwei1987@163.com (J. Xu), xphe@xidian.edu.cn (X. He), drliuqi@scut.edu.cn (Q. Liu).

https://doi.org/10.1016/j.dsp.2023.103942
1051-2004/

effective if there is no range ambiguity. Nevertheless, range ambiguity renders their compensation performance in vain. The reason is that conflicts always occur during clutter compensation for different ambiguous range regions. The direct data domain (DDD) is proposed in [11] and [12]. It can avoid the limitation of range dependence since only single snapshot under test is utilized to estimate the clutter covariance matrix (CCM). However, it suffers the loss of space-time degrees of freedom (DOFs) and thus degrades the performance of clutter suppression and target detection.

To mitigate the problem of range ambiguity, many approaches have been proposed to address the range-ambiguous clutter suppression problem, and they can approximately be classified into two categories, including elevation spatial filtering methods and waveforms diversity methods. For this elevation filtering methods, the central theory is that the elevational DOFs is used to eliminate the near-range clutter. In [13][14][15], a method of elevation filtering is developed to suppress range-ambiguous clutters by using the elevational DOFs provided by a planar array. However, these methods require many DOFs in elevation. In [16][17], some three-dimensional (3-D) STAP approaches are explored, which can null out range-ambiguous clutter to some extent. However, they require many IID training samples to estimate the CCM, which is unavailable in practice. The waveforms diversity method might resolve range ambiguity through modulating the carrier frequency, time delay, and the phase of the transmitted waveforms. The frequency diverse array (FDA) has been developed in [18][19][20][21], which introduces a small frequency increment among adjacent array elements. Thus, the resulting beampattern serves as a function of range, angle, and time. The frequency diverse array with multiple-input multiple-output (FDA-MIMO) radar demonstrates some advantages in many applications. It is shown in [22][23] that, by exploiting the DOFs in the range-angle domain, both range and angle parameters are determined. In [24][25], the problems of mainlobe deceptive jamming are addressed, where the DOFs of range dimension introduced by increment frequency are utilized to distinguish the target and deceptive jamming. In [26][27], adaptive range-angle-Doppler processing approaches are proposed for the FDA-MIMO radar to improve clutter suppression performance, which is capable of distinguishing the range-ambiguous clutter. Note that the resultant multi-dimensional signal processing schemes require a great number of training samples. A range ambiguity resolution approach for high-resolution and wide-swath synthetic aperture radar imaging by using FDA radar is proposed in [28]. In [29], the range-ambiguous clutter is discriminated in the transmitted spatial frequency domain. However, the number of range ambiguity that can be resolved is limited. In [30], the vertical DOFs are developed to apply the frequency diversity, which sufficiently increases the separation performance of range-ambiguous clutters. With this method, the clutter from each ambiguous range region can be extracted and thus the traditional STAP algorithms can be performed on each ambiguous range region. An ambiguous clutter suppression method is proposed in [31] based on transmitted beam main lobe correction for the FDA-MIMO radar. Compared with the traditional FDA radar, it requires no parameter design. In [32], a mainlobe clutter suppression method for blind-Doppler target detection is proposed by exploiting the Doppler-spreading effect in FDA-MIMO radar. In [33], a multi-waveform based on adaptive beamforming in joint transmit-receive (Tx-Rx) domain is proposed for range-ambiguous clutter suppression, where statistical property of primary waveform in Tx-Rx domain can be directly estimated by the multi-waveform data. However, the leverage of Doppler dimensional information is limited. In [34], a slow-time coding scheme based on FDA radar is proposed to separate transmitted DOFs, which is used to separate range-ambiguous clutter. However, the large PRF need to be satisfied for multiple elements system. In [35], a range-ambiguous clutter suppression method based on superimposed stepped frequency (SSF) radar is developed, where range-ambiguous clutter is separated in the carrier frequency domain. It is noted that FDA has wide beampattern coverage compared with its PA counterpart, which results in simultaneously power loss within identical coherent processing interval (CPI).

In this paper, we establish the PA-FDA dual-mode radar in order to maximize the advantages of high beampattern gain of PA and range ambiguity resolvability of FDA. The dual-mode radar consists of two independent parts, i.e., PA and FDA. For the FDA part, the vertical diversity is employed to separate the range-ambiguous clutters. In the sequel, the secondary range dependence compensation and pre-STAP filtering are performed. As range ambiguity is resolved, the CCM corresponding to each range region can be obtained accurately. For the PA part, the CCM corresponding to all ambiguous range regions is obtained by linear combination of CCMs calculated by FDA mode. Moreover, a noise reduction technique is proposed for the linear combination of CCMs in order to mitigate the equivalent noise power in the resultant CCM for PA. The adaptive weight is calculated by using the enhanced CCM in the PA part. The signal-to-clutter-plus-noise ratio (SCNR) is improved due to improved estimation accuracy of CCM and the high beampattern gain of PA mode.

The remainder of this paper is organized as follows. Section 2 introduces the signal model of the PA-FDA dual-mode radar. The range-ambiguous clutter suppression method is presented in Section 3. In Section 4, simulation results are provided to validate the effectiveness of the proposed method. Finally, conclusions are drawn in Section 5.

2. Signal model of PA-FDA dual-mode radar

An airborne forward-looking planar array radar is considered in Cartesian coordinate system, as shown in Fig. 1. The height of the platform is H and the velocity is V. K pulses are transmitted during a CPI. θ and φ denote azimuth and elevation angles of an arbitrary scattering patch, respectively. PRF is $f_{PRF} = 1/T$, with T denoting the pulse-repetition interval. L indicates the number of range bins. Fig. 2 shows the planar array of the dual-mode radar, where N and M stand for the numbers of columns and rows of the planar array, respectively. The PA-FDA dual-mode radar is composed of two parts, i.e., PA and FDA. As shown in Fig. 2, PA part is colored in blue while FDA part is colored in red. PA counterpart transmits M rows coherent waveforms at identical carrier frequencies, and FDA counterpart transmits M rows orthogonal waveforms at different carrier frequencies. $2M$ transmit equivalent phase centers corresponding to PA and FDA part can be obtained, which is located in the midpoints of rows, as shown in the right-hand of Fig. 2. For the receiver, N receive equivalent phase centers situated at the midpoints of columns, as shown in the right-hand of Fig. 2 in black. Therefore, the proposed planar array can be regarded as a cross-array, which has $2M$ transmit elements in vertical and N received elements in horizontal.

PA part: It is pointed that the elevation beampattern of PA is written as

$$G(\varphi_0) = \sum_{m=1}^{M} e^{j2\pi \frac{d(m-1)(\sin\varphi - \sin\varphi_0)}{\lambda_0}} \tag{1}$$

where φ_0 and $\lambda_0 = c/f_0$ are the beam direction and wavelength, respectively.

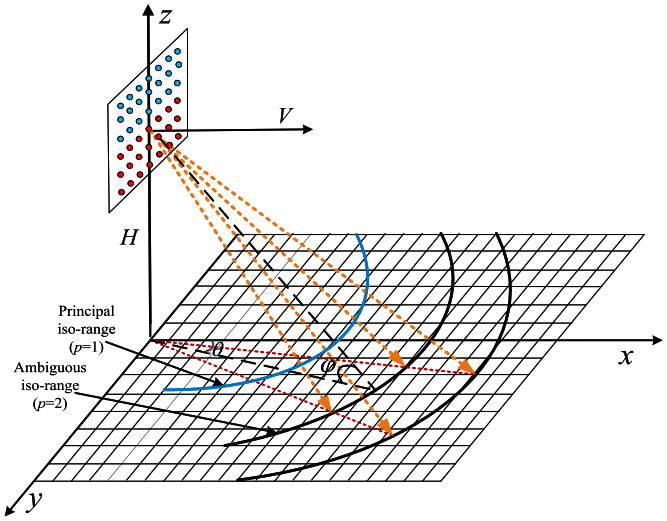

Fig. 1. Geometry of forward-looking planar array radar.

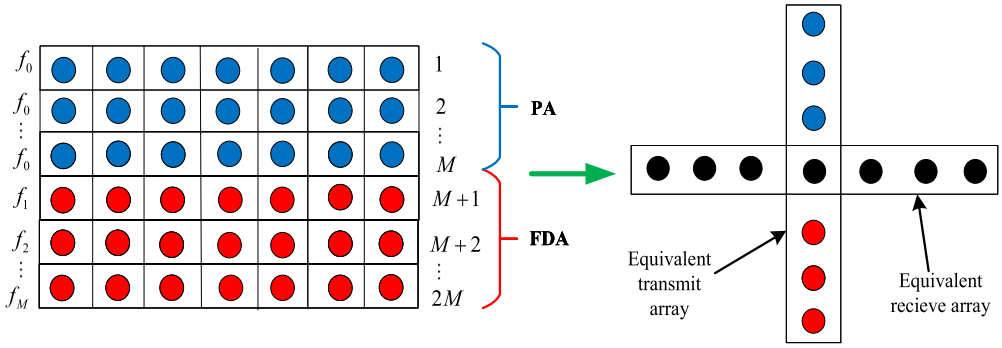

Fig. 2. Planar array and its equivalent transmitting and receiving arrays.

FDA part: The frequency diversity is applied in vertical dimension. Therefore, each row can be treated as one unit with the equivalent phase center positioned at the midpoints of the corresponding rows. Thus, the transmit array is vertical FDA as shown in Fig. 2, i.e., the transmit carrier frequencies vary among equivalent array element in vertical [30], which is expressed as:

$$f_m = f_0 + (m-1)\Delta f \quad m = 1, 2, \cdots M \tag{2}$$

where Δf is frequency increment across two adjacent rows.

Notice that the PA and FDA are operating simultaneously with orthogonal waveforms. i) The transmitted waveform of PA part is denoted as $\Phi_0(t)$. ii) The transmit waveform of FDA part is denoted as $\Phi_m(t)$ for the mth equivalent transmit element. These orthogonal waveforms satisfy:

$$\int_{T_p} \Phi_m(t)\Phi_n^*(t-\tau)e^{j2\pi\Delta f(m-n)t}dt = \delta_{mn}(\tau), \quad m, n = 0, 1, \cdots, M \tag{3}$$

where T_p and τ are the pulse duration and time delay, respectively. $()^*$ denotes the conjugate operation. It is pointed out that ideal orthogonality is unrealistic and the orthogonal waveform optimization is a research topic in radar community [36][37]. In this paper, we still take the orthogonality assumption for simplicity.

In the receive process, each column of the whole planar array is taken as receive subarray. Therefore, there are N received elements with their equivalent phase centers at the midpoints of the corresponding columns. In Fig. 2, the N equivalent received elements are marked as a black point.

Considering an arbitrary clutter scatter corresponding to the lth range bin and pth ambiguous range region as shown in Fig. 1, which is parameterized by slant range $R_{l,p}$, azimuth angle θ_q, and elevation $\varphi_{l,p}$. Thus the round-trip time delay corresponding to PA part is written as

$$\tau^1 = \frac{1}{c}\left\{\begin{array}{l} 2R_{l,p} - \frac{N-1}{2}d\sin(\theta_q)\cos(\varphi_{l,p}) - (M-1)d\sin(\varphi_{l,p}) - (m-1)d\sin(\varphi_{l,p}) \\ -(n-1)d\sin(\theta_q)\cos(\varphi_{l,p}) \end{array}\right\} \tag{4}$$

where c is the speed of light, d is the element spacing. Notice that the reference point is taken as the first element in left-top position. For the FDA part, the round-trip time delay is

$$\tau^2 = \frac{1}{c}\left\{ \begin{array}{l} 2R_{l,p} - \frac{N-1}{2} d\sin\left(\theta_q\right)\cos\left(\varphi_{l,p}\right) - 2\left(M-1\right)d\sin\left(\varphi_{l,p}\right) - \left(m-1\right)d\sin\left(\varphi_{l,p}\right) \\ -\left(n-1\right)d\sin\left(\theta_q\right)\cos\left(\varphi_{l,p}\right) \end{array} \right\} \tag{5}$$

Therefore, the receive signal of the kth pulse and nth received element corresponding to dual-mode radar can be expressed as

$$\begin{aligned} r_{n,k} = &\sum_{m=1}^{M} \xi_{l,p,q} \left\{ \Phi_0\left(t-\tau^1\right) e^{j2\pi f_0\left(t-\tau^1\right)} e^{j2\pi f_{d0}\left(\varphi_{l,p},\theta_q\right)(k-1)} \right\} \\ &+ \sum_{m=1}^{M} \xi_{l,p,q} \left\{ \Phi_m\left(t-\tau^2\right) e^{j2\pi f_m\left(t-\tau^2\right)} e^{j2\pi f_d^m\left(\varphi_{l,p},\theta_q\right)(k-1)} \right\} \end{aligned} \tag{6}$$

where $f_{d0}\left(\varphi_{l,p},\theta_q\right) = 2V f_0 \cos\left(\theta_q\right)\cos\left(\varphi_{l,p}\right)T/c$ represents the normalized Doppler frequency of PA. $f_d^m\left(\varphi_{l,p},\theta_q\right) = 2V f_m \cos\left(\theta_q\right) \times \cos\left(\varphi_{l,p}\right)T/c$ represents the normalized Doppler frequency of FDA. $\xi_{l,p,q}$ is the complex coefficient of the qth scatter corresponding to the lth range bin and pth range-ambiguous region. The down-converting is performed with $e^{j2\pi f_0 t}$, which can be expressed as

$$\begin{aligned} \hat{r}_{n,k} = &\sum_{m=1}^{M} \xi_{l,p,q} \Phi_0\left(t-\tau^1\right) e^{-j2\pi f_0 \tau^1} e^{j2\pi f_{d0}\left(f_{d0}\left(\varphi_{l,p},\theta_q\right)\right)(k-1)} \\ &+ \sum_{m=1}^{M} \xi_{l,p,q} \Phi_m\left(t-\tau^2\right) e^{j2\pi \Delta f t} e^{-j2\pi f_m \tau^2} e^{j2\pi f_d^m\left(f_{d0}\left(\varphi_{l,p},\theta_q\right)\right)(k-1)} \end{aligned} \tag{7}$$

In the following, the matched filtering is implemented with $h(t) = \Phi_0(t)$, which can be expressed as

$$\begin{aligned} r_{n,k}^{PA} &= r_{n,k} \circledast h(t) = \int r_{n,k}\left(\tau-\tau^1\right)\Phi_0^*(\tau - t)\, d\tau \\ &= \sum_{m=1}^{M} \xi_{l,p,q}\delta\left(t-\tau_0\right) e^{-j2\pi f_0\tau^1} e^{j2\pi f_{d0}\left(f_{d0}\left(\varphi_{l,p},\theta_q\right)\right)(k-1)} \\ &= \xi_{l,p,q} e^{-j2\pi \frac{f_0}{c}\left(2R_{l,p} - \frac{N-1}{2}d\sin\left(\theta_q\right)\cos\left(\varphi_{l,p}\right) - Md\sin\left(\varphi_{l,p}\right)\right)} e^{j2\pi f_{d0}\left(f_{d0}\left(\varphi_{l,p},\theta_q\right)\right)(k-1)} \\ &\quad \times e^{-j2\pi \frac{f_0}{c}(n-1)d\sin\left(\theta_q\right)\cos\left(\varphi_{l,p}\right)} \sum_{m=1}^{M} e^{-j2\pi \frac{f_0}{c}(m-1)d\sin\left(\varphi_{l,p}\right)} \end{aligned} \tag{8}$$

where $\circledast$ denotes the convolution operator. The narrow band approximation is used, i.e., $\Phi_0\left(t-\tau^1\right) \approx \Phi_0\left(t-\tau_0\right) = \Phi_0\left(t-2R_{l,p}/c\right)$. Note that the FDA signal has been removed by waveforms orthogonality, i.e.,

$$\sum_{m=1}^{M} \xi_{l,p,q} e^{j2\pi \Delta f t} e^{-j2\pi f_m \tau^2} e^{j2\pi f_d^m\left(f_{d0}\left(\varphi_{l,p},\theta_q\right)\right)(k-1)} \int \Phi_m\left(\tau-\tau^2\right)\Phi_0^*(\tau - t)\, d\tau = 0 \tag{9}$$

The constant complex term $e^{-j2\pi \frac{f_0}{c}\left(2R_{l,p} - \frac{N-1}{2}d\sin\left(\theta_q\right)\cos\left(\varphi_{l,p}\right) - Md\sin\left(\varphi_{l,p}\right)\right)}$ is incorporated into complex coefficient $\xi_{l,p,q}$. By straightforward mathematical manipulation for (8), we can obtain the simplified received clutter signal of the particular patch corresponding to the PA part, that is,

$$r_{n,k}^{PA}\left(\varphi_{l,p},\theta_q\right) = \xi_{l,p,q} G\left(\varphi_{l,p}\right) e^{j2\pi\left[f_h\left(\varphi_{l,p},\theta_q\right)(n-1) + f_{d0}\left(\varphi_{l,p},\theta_q\right)(k-1)\right]} \tag{10}$$

where $f_h\left(\varphi_{l,p},\theta_q\right) = d\sin\left(\theta_q\right)\cos\left(\varphi_{l,p}\right)/\lambda_0$ is the receive spatial frequency. The received clutter signal of all N-element and K-pulse is stacked into a vector form as

$$\begin{aligned} \boldsymbol{y}^{PA}\left(\varphi_{l,p},\theta_q\right) &= \left[\, r_{1,1}^{PA}\left(\varphi_{l,p},\theta_q\right) \quad \cdots \quad r_{N,K}^{PA}\left(\varphi_{l,p},\theta_q\right) \,\right]^T \\ &= \xi_{l,p,q} G\left(\varphi_{l,p}\right) \boldsymbol{\alpha}_h\left(f_h\left(\varphi_{l,p},\theta_q\right)\right) \otimes \boldsymbol{\beta}\left(f_{d0}\left(\varphi_{l,p},\theta_q\right)\right) \end{aligned} \tag{11}$$

where $\otimes$ is the Kronecker product. $\boldsymbol{\alpha}_h\left(f_h\left(\varphi_{l,p},\theta_q\right)\right) \in {}^{N\times 1}$ and $\boldsymbol{\beta}\left(f_{d0}\left(\varphi_{l,p},\theta_q\right)\right) \in {}^{K\times 1}$ are the receive spatial steering vector and temporal steering vector, respectively. They are written as

$$\boldsymbol{\alpha}_h\left(f_h\left(\varphi_{l,p},\theta_q\right)\right) = \left[\, 1 \quad e^{j2\pi f_h\left(\varphi_{l,p},\theta_q\right)} \quad \ldots \quad e^{j2\pi f_h\left(\varphi_{l,p},\theta_q\right)(N-1)} \,\right]^T \tag{12}$$

$$\boldsymbol{\beta}\left(f_{d0}\left(\varphi_{l,p},\theta_q\right)\right) = \left[\, 1 \quad e^{j2\pi f_{d0}\left(\varphi_{l,p},\theta_q\right)} \quad \ldots \quad e^{j2\pi f_{d0}\left(\varphi_{l,p},\theta_q\right)(K-1)} \,\right]^T \tag{13}$$

where the superscript ^{T} denotes the transpose operator. Note that $G\left(\varphi_{l,p}\right)$ denotes the transmit gain of PA.

On the other hand, we can obtain the simplified received clutter signal of the particular patch corresponding to the FDA part. Since FDA transmits orthogonal waveforms with each transmit element, we obtain the echoes corresponding to the mth transmit element, nth receive element, and kth pulse as:

$$r_{m,n,k}^{FDA}\left(R_{l,p},\varphi_{l,p},\theta_q\right)=\xi_{l,p,q}e^{j2\pi\left[f_t\left(R_{l,p},\varphi_{l,p}\right)+\Delta f_v\left(\varphi_{l,p}\right)(m-1)\right](m-1)}e^{j2\pi\left[f_h\left(\varphi_{l,p},\theta_q\right)+\Delta f_h\left(\varphi_{l,p},\theta_q\right)(m-1)\right](n-1)} \times e^{j2\pi\left[f_{d0}\left(\varphi_{l,p},\theta_q\right)+\Delta f_d\left(\varphi_{l,p},\theta_q\right)(m-1)\right](k-1)} \tag{14}$$

where $f_t\left(R_{l,p},\varphi_{l,p}\right)=f_r\left(R_{l,p}\right)+f_v\left(\varphi_{l,p}\right)$ is the transmit vertical spatial frequency, $f_r=-2\Delta f R_{l,p}/c$ and $f_v=d\sin\left(\varphi_{l,p}\right)/\lambda_0$ are the range frequency and vertical spatial frequency, respectively. $\Delta f_d\left(\varphi_{l,p},\theta_q\right)=2VT\Delta f\cos\left(\varphi_{l,p}\right)\cos\left(\theta_q\right)/c$, $\Delta f_v\left(\varphi_{l,p}\right)=\Delta f d\sin\left(\varphi_{l,p}\right)/c$ and $\Delta f_h=\Delta f d\sin\left(\theta_q\right)\cos\left(\varphi_{l,p}\right)/c$ are the additional Doppler frequency, transmit spatial frequency and receive spatial frequency, respectively. These additional frequency terms are negligible under the condition of $\Delta f\ll f_0$ [30]. Thus (14) can be further expressed as

$$r_{m,n,k}^{FDA}\left(R_{l,p},\varphi_{l,p},\theta_q\right)=\xi_{l,p,q}e^{j2\pi f_t\left(R_{l,p},\varphi_{l,p}\right)(m-1)}e^{j2\pi f_h\left(\varphi_{l,p},\theta_q\right)(n-1)}e^{j2\pi f_{d0}\left(\varphi_{l,p},\theta_q\right)(k-1)} \tag{15}$$

Here $\xi_{l,p,q}$ incorporates the whole constant exponential phase terms. Therefore, the received signal of clutter scatter in the transmit, receive and temporal dimensions can be written as

$$\begin{aligned}\boldsymbol{y}^{FDA}\left(R_{l,p},\varphi_{l,p},\theta_q\right)&=\left[\begin{array}{ccc}r_{1,1,1}^{FDA}\left(R_{l,p},\varphi_{l,p},\theta_q\right) & \cdots & r_{M,N,K}^{FDA}\left(R_{l,p},\varphi_{l,p},\theta_q\right)\end{array}\right]\\&=\xi_{l,p,q}\,\boldsymbol{\alpha}_v\left(f_t\left(R_{l,p},\varphi_{l,p}\right)\right)\otimes\boldsymbol{\alpha}_h\left(f_h\left(\varphi_{l,p},\theta_q\right)\right)\otimes\boldsymbol{\beta}\left(f_{d0}\left(\varphi_{l,p},\theta_q\right)\right)\end{aligned} \tag{16}$$

where $\boldsymbol{\alpha}_v\left(f_t\left(R_{l,p},\varphi_{l,p}\right)\right)$ is the transmit steering vector, which can be expressed as

$$\boldsymbol{\alpha}_v\left(f_t\left(R_{l,p},\varphi_{l,p}\right)\right)=\left[\begin{array}{cccc}1 & e^{j2\pi f_t\left(R_{l,p},\varphi_{l,p}\right)} & \cdots & e^{j2\pi f_t\left(R_{l,p},\varphi_{l,p}\right)(M-1)}\end{array}\right]^T \tag{17}$$

The transmit spatial frequency is dependent on the range parameter, indicating that FDA-MIMO radar provides additional controllable DOFs in the range domain. This enables FDA to address range-ambiguity problem. As a summary, the total received signal of PA-FDA dual-mode radar can be expressed as

$$\begin{aligned}\boldsymbol{y}^{PA-FDA}\left(R_{l,p},\varphi_{l,p},\theta_q\right)&=\left[\begin{array}{c}\boldsymbol{y}^{PA}\left(\varphi_{l,p},\theta_q\right)\\ \boldsymbol{y}^{FDA}\left(R_{l,p},\varphi_{l,p},\theta_q\right)\end{array}\right]\\&=\xi_{l,p,q}\left[\begin{array}{c}G\left(\varphi_{l,p}\right)\\ \boldsymbol{\alpha}_v\left(f_t\left(R_{l,p},\varphi_{l,p}\right)\right)\end{array}\right]\otimes\boldsymbol{\alpha}_h\left(f_h\left(\varphi_{l,p},\theta_q\right)\right)\otimes\boldsymbol{\beta}\left(f_{d0}\left(\varphi_{l,p},\theta_q\right)\right)\end{aligned} \tag{18}$$

Notice that the complex-valued reflection coefficients of PA and FDA differ by an exponential phase in (11) and (16). Nevertheless, the exponential phase can be merged to $G\left(\varphi_{l,p}\right)$, which has no influence for further processing.

The ground clutter echo of the lth range bin is the coherent summation of many scatters within the bound of the iso-range in the case of range ambiguity, which is expressed as

$$\begin{aligned}\boldsymbol{c}_l&=\sum_{p=1}^{N_a}\sum_{q=1}^{N_c}\boldsymbol{y}^{PA-FDA}\left(R_{l,p},\varphi_{l,p},\theta_q\right)\\&=\sum_{p=1}^{N_a}\sum_{q=1}^{N_c}\xi_{l,p,q}\left[\begin{array}{c}G\left(\varphi_{l,p}\right)\\ \boldsymbol{\alpha}_v\left(f_t\left(R_{l,p},\varphi_{l,p}\right)\right)\end{array}\right]\otimes\boldsymbol{\alpha}_h\left(f_h\left(\varphi_{l,p},\theta_q\right)\right)\otimes\boldsymbol{\beta}\left(f_{d0}\left(\varphi_{l,p},\theta_q\right)\right)\end{aligned} \tag{19}$$

where N_a denotes the number of range ambiguity, N_c is the number of statistically independent clutter scatters within the single range bin. Generally, the received echoes are composed by the clutter, target and noise, which is expressed as

$$\boldsymbol{x}_l=\boldsymbol{c}_l+\boldsymbol{s}_l+\boldsymbol{n}_l \tag{20}$$

where $\boldsymbol{c}_l$, $\boldsymbol{s}_l$ and $\boldsymbol{n}_l$ represent the clutter, target and additive Gaussian white noise, respectively. Considering a moving target with complex coefficient ε_0, the target signal can be written as

$$\boldsymbol{s}_l=\varepsilon_0\hat{\boldsymbol{\gamma}}\left(R_0,\varphi_0,\theta_0,v_0\right)=\varepsilon_0\left[\begin{array}{c}G\left(\varphi_0\right)\\ \boldsymbol{\alpha}_v\left(f_t\left(R_0,\varphi_0\right)\right)\end{array}\right]\otimes\boldsymbol{\alpha}_h\left(f_h\left(\varphi_0,\theta_0\right)\right)\otimes\boldsymbol{\beta}\left(f_{dt}\left(\varphi_0,\theta_0,v_0\right)\right) \tag{21}$$

where $\hat{\boldsymbol{\gamma}}\left(R_l,\varphi_0,\theta_0,v_0\right)$ is the presumed space-time-range steering vector of the target, where R_0, θ_0, φ_0 and v_0 are the range, azimuth angle, elevation angle and radial velocity of the target, respectively. Here $f_{dt}\left(\varphi_0,\theta_0,v_0\right)=2\left(V\cos\left(\theta_0\right)\cos\left(\varphi_0\right)+v_0\right)T/\lambda_0$ is the normalized Doppler frequency of the target.

3. Clutter suppression scheme of dual-mode radar

In this section, a clutter suppression scheme for PA-FDA dual mode radar is presented. It is known that the conventional PA radar suffers sufficient performance loss in range-ambiguous clutter scenario. In contrast, FDA is superior in range ambiguous clutter separation. The proposed scheme contains two key points: i) The range-ambiguous clutters are separated by using FDA, and ii) A reconstructed CCM is applied for range-ambiguous clutter suppression for PA.

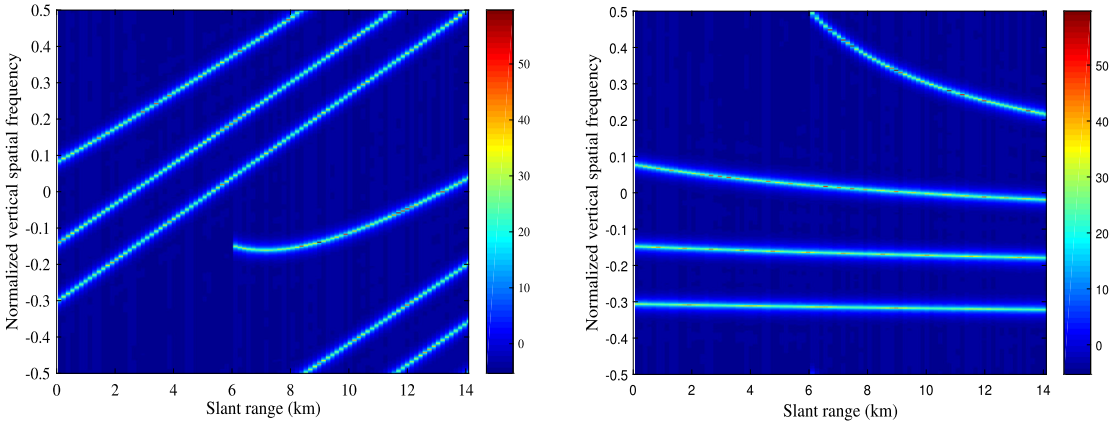

Fig. 3. Clutter spectrum in vertical spatial frequency-range domain for FDA radar (a) Before SRDC (b) After SRDC.

3.1. Range-ambiguous clutter separation with FDA

In the vertical FDA counterpart, the range-ambiguous clutter can be completely separated in the vertical spatial frequency domain by introducing range frequency. To better separate and extract rang-ambiguous clutters, secondary range dependence compensation (SRDC) and pre-STAP filtering are required [30].

The transmit vertical spatial frequency of FDA in (14) is defined as follows

$$\begin{aligned} f_t\left(R_{l,p},\varphi_{l,p}\right) &= f_r\left(R_{l,p}\right)+f_v\left(\varphi_{l,p}\right) = -\frac{2\Delta f R_{l,p}}{c}+\frac{d\sin\left(\varphi_{l,p}\right)}{\lambda_0} \\ &= -\frac{2\Delta f}{c}R_l-\frac{2\Delta f}{c}\left(p-1\right)R_u+\frac{dH}{\lambda_0 R_{l,p}} \end{aligned} \tag{22}$$

where $R_{l,p}=R_l+(p-1)R_u$ denotes the slant range of clutter located in the pth range-ambiguous region within the lth range bin, R_l is the principal slant range, R_u is the maximum unambiguous range, and $\sin\left(\varphi_{l,p}\right)=H/R_{l,p}$.

Compared with the vertical spatial frequency of traditional PA, the range frequency $f_r\left(R_{l,p}\right)$ is an extra term due to the increment frequency Δf. We can see from (22) that the range frequency $f_r\left(R_{l,p}\right)$ is function of the principal slant range R_l and index of the range ambiguity p. As R_l is known for each range bin, the compensation vector is constructed as [30]:

$$\boldsymbol{h}_c\left(R_l\right)=\left[\begin{array}{cccc}1 & e^{j4\pi\frac{\Delta f}{c}R_l} & \cdots & e^{j4\pi\frac{\Delta f}{c}R_l(M-1)}\end{array}\right]^T \tag{23}$$

After SRDC, the 3-D clutter snapshot of FDA in the range bin can be expressed as

$$\boldsymbol{c}_l^{FDA}=\sum_{p=1}^{N_a}\sum_{q=1}^{N_c}\xi_{l,p,q}\,\tilde{\boldsymbol{\alpha}}_v\left(f_t\left(R_{l,p},\varphi_{l,p}\right)\right)\otimes\boldsymbol{\alpha}_h\left(f_h\left(\varphi_{l,p},\theta_q\right)\right)\otimes\boldsymbol{\beta}\left(f_{d0}\left(\varphi_{l,p},\theta_q\right)\right) \tag{24}$$

where $\tilde{\boldsymbol{\alpha}}_v\left(f_t\left(R_{l,p},\varphi_{l,p}\right)\right)=\boldsymbol{h}_c\left(R_l\right)\odot\boldsymbol{\alpha}_v\left(f_t\left(R_{l,p},\varphi_{l,p}\right)\right)$ is the compensated transmit steering vector. The compensated vertical spatial frequency can be expressed as

$$\tilde{f}_t\left(p,\varphi_{l,p}\right)=-\frac{2\Delta f}{c}\left(p-1\right)R_u+\frac{d\sin\left(\varphi_{l,p}\right)}{\lambda_0} \tag{25}$$

Fig. 3(a) and Fig. 3(b) depict the power spectrum of range ambiguous clutters in the vertical spatial frequency domain before and after SRDC, respectively. Here we consider the range ambiguous number as 4. It is observed that the power spectra change evidently with respect to slant range in Fig. 3(a) while the variation is alleviated after SRDC in Fig. 3(b). Therefore, it is possible to separate the range ambiguous clutter in the transmit vertical spatial frequency domain by designing a series of bandpass spatial filters, referred to as pre-STAP filters.

The pre-STAP filtering is applied to extract clutters from different range-ambiguous regions, which is express as

$$\boldsymbol{g}_p=\left[\begin{array}{cccc}1 & e^{j2\pi\tilde{f}_t\left(p,\varphi_{l,p}\right)} & \cdots & e^{j2\pi\tilde{f}_t\left(p,\varphi_{l,p}\right)(M-1)}\end{array}\right]^T \tag{26}$$

Notice that low-sidelobe property is desired for the pre-STAP filters in practice. The extracted clutter corresponding to the pth range-ambiguous region in the lth range bin can be expressed as:

$$\boldsymbol{c}_{l,p}^{FDA}=\sum_{p=1}^{N_a}\sum_{q=1}^{N_c}\xi_{l,p,q}\left[\boldsymbol{g}_p^H\tilde{\boldsymbol{\alpha}}_v\left(f_t\left(R_{l,p},\varphi_{l,p}\right)\right)\right]\otimes\boldsymbol{\alpha}_h\left(f_h\left(\varphi_{l,p},\theta_q\right)\right)\otimes\boldsymbol{\beta}\left(f_{d0}\left(\varphi_{l,p},\theta_q\right)\right) \tag{27}$$

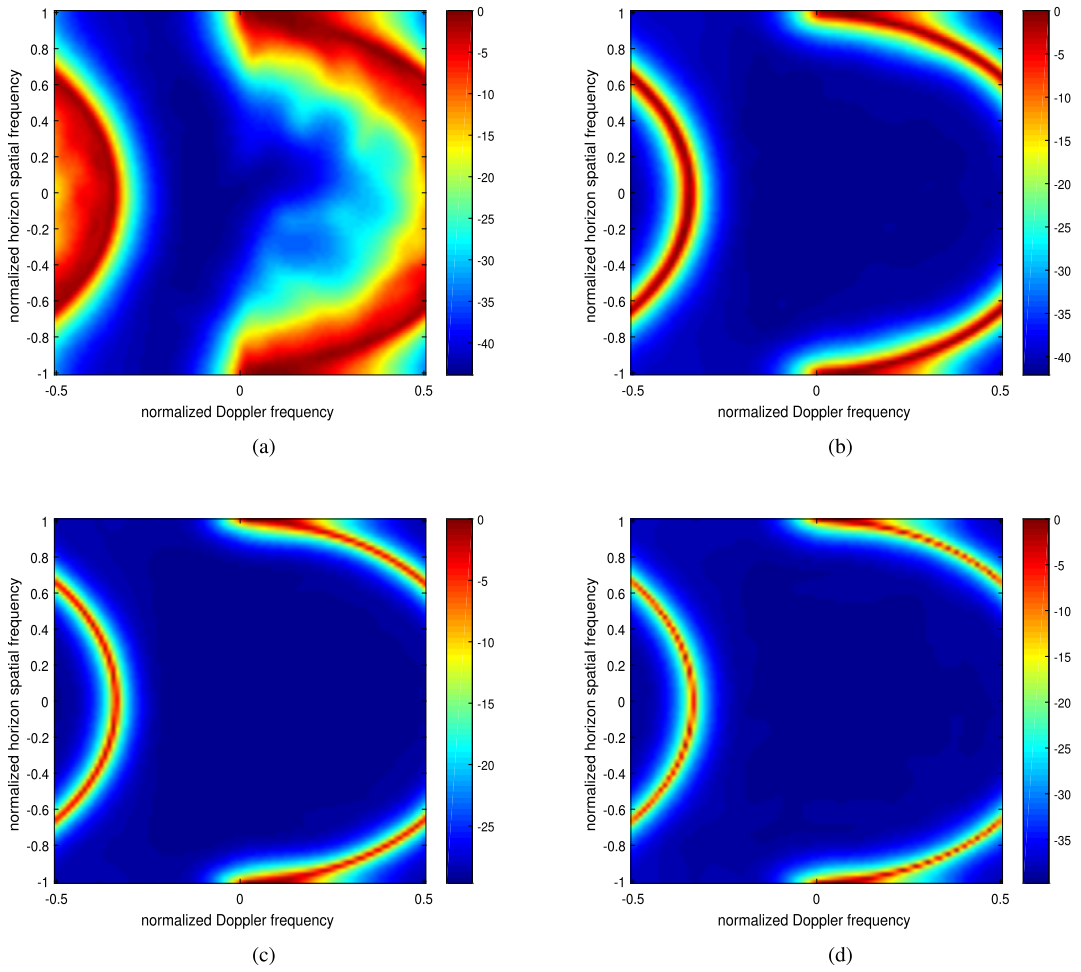

Fig. 4. Separated clutter spectrum distribution for each ambiguous range region (a) First range region (b) Second range region (c) Third range region (d) Fourth range region.

It follows from (27) that the clutter in vertical spatial dimensional is filtered, i.e., $\boldsymbol{g}_p^H \tilde{\boldsymbol{\alpha}}_v \left(f_t\left(R_{l,p}, \varphi_{l,p}\right)\right)$. The pre-STAP is equivalent to beamforming in vertical dimension.

The power spectra of separated range ambiguous clutters for the airborne forward-looking array radar are plotted in Fig. 4. Here we consider the range ambiguous number as 4. It is observed that the clutter spectrum of the first range-ambiguous region is severely spread due to range dependence of the near-range clutter. In contrast, the range dependence of the second, third, and fourth range regions is not so serious. Basically, the separation of range ambiguous clutters enables range dependence compensation for the first range region independently.

In the sequel, the range dependence compensation approach can be applied, especially for the first range region echo. Here we use the DW method [5] as an example, which is written as

$$\hat{\boldsymbol{c}}_{l,p}^{FDA} = e^{j2\pi(k-1)\Delta f_D^{l,p}} \boldsymbol{c}_{l,p}^{FDA} \tag{28}$$

where $\Delta f_D^{l,p}$ is the Doppler frequency difference between the lth range cell and the cell under test (CUT) within the pth range-ambiguous region. Therefore, the CCMs corresponding to each range regions can be estimated independently with maximum likelihood approach, that is,

$$\boldsymbol{R}_{l_0,p}^{FDA} = E\left[\left(\hat{\boldsymbol{c}}_{l,p}^{FDA}\right)\left(\hat{\boldsymbol{c}}_{l,p}^{FDA}\right)^H\right] \approx \frac{1}{L-1}\sum_{l=1, l\neq l_0}^{L}\left(\hat{\boldsymbol{c}}_{l,p}^{FDA}\right)\left(\hat{\boldsymbol{c}}_{l,p}^{FDA}\right)^H \tag{29}$$

where l_0 is the range bin where the target dwells.

3.2. Range-ambiguous clutter suppression for PA counterpart

Recall that PA radar suffers serious performance degradation of clutter suppression due to the existence of range dependence and range ambiguity for the forward-looking geometry. The CCM of PA part in the l_0th range bin can be written as

$$\boldsymbol{R}_{l_0}^{PA} = E\left[\left(\boldsymbol{c}_{l_0}^{PA}\right)\left(\boldsymbol{c}_{l_0}^{PA}\right)^H\right] = E\left[\left(\sum_{p=1}^{N_a}\boldsymbol{c}_{l_0,p}^{PA}\right)\left(\sum_{p=1}^{N_a}\boldsymbol{c}_{l_0,p}^{PA}\right)^H\right] = E\left[\sum_{p=1}^{N_a}\left(\boldsymbol{c}_{l_0,p}^{PA}\right)\left(\boldsymbol{c}_{l_0,p}^{PA}\right)^H\right] = \sum_{p=1}^{N_a}\boldsymbol{R}_{l_0,p}^{PA} \tag{30}$$

Notice that it is impossible to calculate $\boldsymbol{R}_{l_0,p}^{PA}$ because range ambiguous echoes cannot be separated in the PA part. Nevertheless, under specific conditions, the covariance matrix corresponding to each range bin of PA part can be represented with that of the FDA part, because they share the same spatial and temporal structures. Fortunately, the range ambiguous clutter echoes can be separated with pre-STAP filters and the distinct CCMs can be calculated by (29). Therefore, the accurate CCMs estimated by FDA part can be applied in the PA counterpart to address the CCM estimation issue. By combining the PA and FDA advantages, it is possible to handle range ambiguous clutter suppression problem for forward-looking geometry.

Basically, the CCM corresponding to the PA counterpart is represented by linearly combining the distinct CCMs of different ambiguous range regions, that is

$$\boldsymbol{R}_{l_0}^{c} = \sum_{p=1}^{N_a} \boldsymbol{R}_{l_0,p}^{FDA} \tag{31}$$

As the linear combination increases the equivalent noise power, we further applied the noise reduction method by calculating the equivalent noise power within the reconstructed covariance matrix. The eigenvalue spectrum is utilized to analyze the noise power of the CCM. The eigenvalue decomposition of $\boldsymbol{R}_{l_0}^{c}$ is written as

$$\boldsymbol{R}_{l_0}^{c} = \boldsymbol{V}\boldsymbol{\Lambda}\boldsymbol{V}^{H} = \sum_{i=1}^{NK} \lambda_i \boldsymbol{v}_i \boldsymbol{v}_i^{H} \tag{32}$$

where $\boldsymbol{\Lambda} = diag\left(\begin{array}{cccc}\lambda_1 & \lambda_2 & \cdots & \lambda_{NK}\end{array}\right)$ is a diagonal matrix with each entry being the eigenvalue of the covariance matrix, and $\boldsymbol{V} = \left[\begin{array}{cccc} v_1 & v_2 & \cdots & v_{NK}\end{array}\right]$ is the matrix containing all the eigenvectors. The eigenvalues are organized in non-increasing order as

$$\lambda_1 > \lambda_2 > \cdots \lambda_h > \lambda_{h+1} \approx \cdots \approx \lambda_{NK} \tag{33}$$

where h is the clutter DOF under range ambiguous clutter scenario, which is studied in [38]. However, due to non-ideal array configuration and system errors, the rank of clutter subspace is difficult to determine. To address this problem, a random matrix theory-minimum description length (RMT-MDL) is applied to estimate clutter DOFs in [39]. Firstly, the density function (PDF) of the test statistics is created as:

$$f\left(t_c\left(h\right)|\hat{\boldsymbol{\theta}}\right) = \frac{1}{\sqrt{4\pi u^2}} \exp\left[-\frac{\left(t_c\left(h\right)\right)^2}{4u^2}\right] u \tag{34}$$

where $t_c\left(h\right)$ is test statistics. $\hat{\boldsymbol{\theta}}$ is the maximum likelihood estimation of eigenvalue vector, and $u = NK/L$. Moreover, according to the MDL criterion, the MDL of the data matrix $\boldsymbol{X}$ is expressed as

$$\Lambda\left(\boldsymbol{X}|\hat{\boldsymbol{\theta}}\right) = -\ln\left\{f\left(t_c\left(h\right)|\hat{\boldsymbol{\theta}}\right)\right\} + \frac{1}{2}\left(h+1\right)\ln L \tag{35}$$

where $\boldsymbol{X} = \left[\begin{array}{ccccc}\boldsymbol{x}_1 & \boldsymbol{x}_2 & \cdots & \boldsymbol{x}_l & \cdots & \boldsymbol{x}_L\end{array}\right]$ is data matrix. Take (35) as the cost function, the simplified clutter DOFs h estimation is expressed as

$$\hat{h} = \underset{h\in(0,NK)}{\arg\min}\left\{\frac{1}{4u^2}\left[\frac{\left(NK-h\right)\sum\limits_{i=h+1}^{NK}\lambda_i^2}{\left(\sum\limits_{i=h+1}^{NK}\lambda_i\right)^2} - \left(1+u\right)\right] + \frac{\left(h+1\right)\ln L}{2}\right\} \tag{36}$$

The noise power is calculated as

$$\sigma_n^2 = \frac{1}{NK-\hat{h}}\sum_{i=\hat{h}}^{NK}\lambda_i \tag{37}$$

Therefore, the reconstructed covariance matrix is updated as

$$\widehat{\boldsymbol{R}}_{l_0}^{c} = \boldsymbol{R}_{l_0}^{c} - \sigma_n^2\boldsymbol{I} \tag{38}$$

where $\boldsymbol{I}$ is the identity matrix, and σ_n^2 is the estimated noise power.

We compared several different methods with RMT-MDL method in Fig. 5(a), including ideal case in [40], principal component analysis (PCA). It is obviously observed that the power of infection point estimated by both ideal case and PCA is significant large. Therefore, neither ideal case nor PCA method can obtain relatively accurate estimation of clutter DOFs. In Fig. 5(b), the eigenvalue curves of the covariance matrices before and after noise reduction are plotted. Besides, the eigenvalue curves of the covariance matrices corresponding to the first and second range regions are provided as comparison. Before noise reduction as in (31), the noise power is increased obviously. In contrast, the noise reduction method in (38) can reduce the noise power sufficiently.

For the moving target at l_0th range bin, the adaptive optimal weight is calculated based on the minimum variance distortionless response (MVDR) criterion, that is

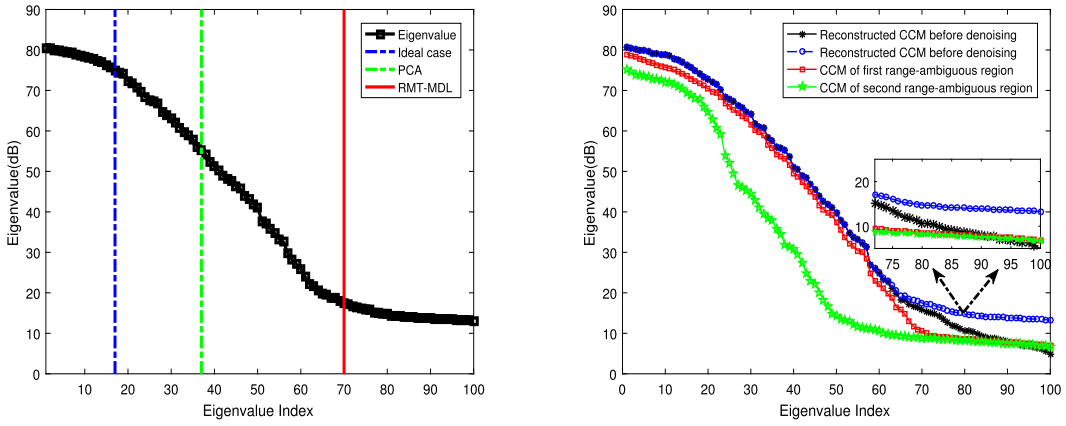

Fig. 5. Eigenvalue spectra (a) Comparison of clutter DOFs estimation (b) Eigenvalue spectra corresponding to different covariance matrices.

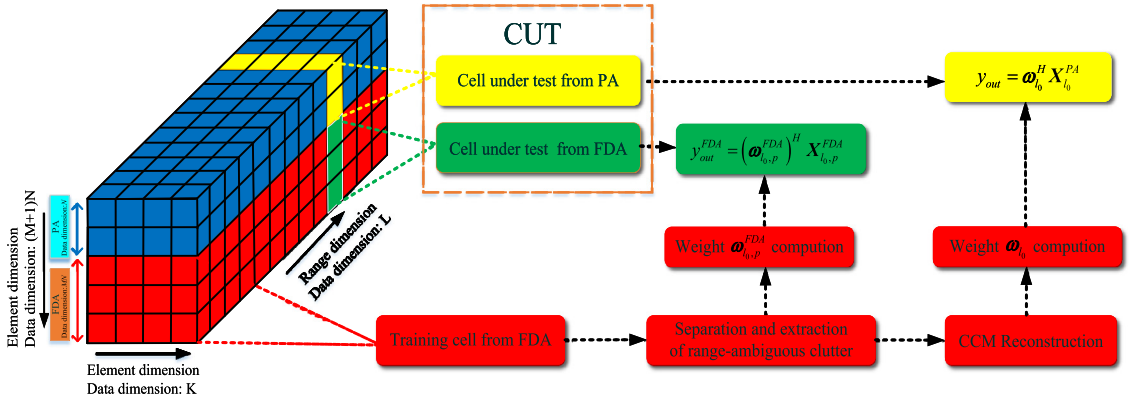

Fig. 6. Procedure of target detection for PA-FDA dual mode radar.

$$\boldsymbol{\omega}_{l_0} = \frac{\left(\hat{\boldsymbol{R}}_{l_0}^{c}\right)^{-1}\tilde{\boldsymbol{t}}\left(\theta_0, \varphi_0, v_0\right)}{\tilde{\boldsymbol{t}}^{H}\left(\theta_0, \varphi_0, v_0\right)\left(\hat{\boldsymbol{R}}_{l_0}^{c}\right)^{-1}\tilde{\boldsymbol{t}}\left(\theta_0, \varphi_0, v_0\right)} \tag{39}$$

where $\tilde{\boldsymbol{t}}\left(\theta_0, \varphi_0, v_0\right) = \boldsymbol{\alpha}_h\left(f_h\left(\varphi_0, \theta_0\right)\right) \otimes \boldsymbol{\beta}\left(f_{dt}\left(\varphi_0, \theta_0, v_0\right)\right)$ is the space-time steering of the target. $\boldsymbol{\alpha}_h\left(f_h\left(\varphi_0, \theta_0\right)\right)$ $\boldsymbol{\beta}\left(f_{dt}\left(\varphi_0, \theta_0, v_0\right)\right)$ are the temporal and spatial steering vectors, respectively. The SCNR output corresponding to the CUT of the PA counterpart is written as

$$\tilde{y}_{out} = \boldsymbol{\omega}_{l_0}^{H}\boldsymbol{x}_{l_0}^{PA} \tag{40}$$

where $\boldsymbol{x}_{l_0}^{PA}$ is the dual-mode radar data of the l_0th range bin corresponding to the PA part.

Note that the FDA part can simultaneously search for the targets located in the other angle regions by employing the wide beam coverage property when the PA part detects and tracks the mainlobe target. For the target located in the other angle region from pth range region, the adaptive optimal weight is calculated using the CCM estimated by FDA, that is

$$\boldsymbol{\omega}_{l_0,p}^{FDA} = \frac{R_{l_0,p}^{FDA}\tilde{t}\left(\theta_1, \varphi_1, v_1\right)}{\tilde{t}^{H}\left(\theta_1, \varphi_1, v_1\right)\left(R_{l_0,p}^{FDA}\right)^{-1}\tilde{t}\left(\theta_1, \varphi_1, v_1\right)} \tag{41}$$

where v_1 represents the speed of target located in the other angle region. The target SCNR output is calculated as

$$y_{out}^{FDA} = \left(\boldsymbol{\omega}_{l_0,p}^{FDA}\right)^{H}\boldsymbol{X}_{l_0,p}^{FDA} \tag{42}$$

where $X_{l_0,p}^{FDA}$ stands for the data received by FDA part in the l_0th range bin.

The received echo structure of the PA-FDA dual-mode radar is depicted in Fig. 6. Here we plot the echo structure after transmit waveforms separation. The 3-D cubic data matrix is composed of upper and lower portions, where the upper part in blue is PA data and the lower part in red is FDA data. Thus there are equivalent MN entries in element dimension corresponding to FDA part. In contrast, there are N entries in element dimension corresponding to PA part. There are K entries in pulse dimension. Specifically, the data blocks in yellow and green belong to the data under test from PA and FDA part, respectively.

The main procedure of moving target detection can be depicted in Fig. 6. Firstly, clutters from different ambiguous range regions are separated in FDA part by performing SDRC and pre-STAP filtering. Secondly, accurate CCMs corresponding to ambiguous range regions are

Table 1
Radar parameters for the simulated data.

Parameters	Values
Platform height	6000 m
Platform speed	500 m/s
Array element spacing	0.075 m
Frequency increment	-8750 Hz
PRF	10000 Hz
Transmitted channel of vertical FDA	17
Transmitted channel of vertical PA	17
Received channel	10
Pulse number	10
Clutter-to-noise ratio	50

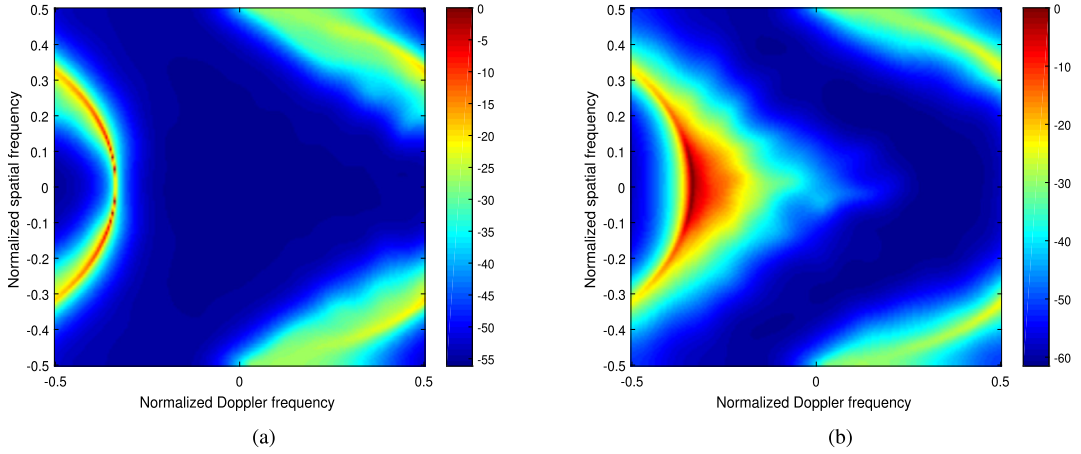

Fig. 7. Clutter spectrum compensated by DW (a) without range ambiguity (b) with range ambiguity.

estimated with further employing range dependence compensation. Thirdly, the CCM of PA part is reconstructed by linearly combining the CCMs estimated by FDA part. Finally, the adaptive weight is computed to suppress the range-ambiguous clutter for the PA part. Moreover, the dual-mode radar can also leverage target detection within large angular coverage as FDA has wide spatial coverage.

4. Simulation results

In this section, simulation results are provided to verify the effectiveness of the proposed method. The system parameters of the PA-FDA dual-mode radar are listed in Table 1.

4.1. Clutter spectra of traditional PA radar in range-ambiguous clutter

The DW method is adopted to compensate clutter range dependence caused by the array geometry of non-side looking in this paper. The clutter spectra compensated by the DW method without and with range ambiguity are presented in Fig. 7(a) and Fig. 7(b), respectively. It is observed from Fig. 7(a) that the clutter spectrum is well focused by the DW compensation, while the clutter spectrum is severely spread in the presence of range ambiguity, which dramatically degrades target detection performance, especially for slow-moving targets.

4.2. Analysis of clutter suppression in PA-FDA radar

The signal-to-clutter-plus-noise ratio (SCNR) loss factor is commonly employed to evaluate the detection performance of the STAP radar. The SCNR loss factor is defined as the ratio of clutter-limited output SCNR to the noise-limited output SNR, i.e.,

$$SCNR_{loss} = \frac{SCNR_{out}}{SNR_{out}} = \frac{\frac{\boldsymbol{\omega}^H \boldsymbol{R}_s \boldsymbol{\omega}}{\boldsymbol{\omega}^H \boldsymbol{R}_{c+n} \boldsymbol{\omega}}}{\frac{\boldsymbol{\omega}^H \boldsymbol{R}_s \boldsymbol{\omega}}{\boldsymbol{\omega}^H \boldsymbol{R}_n \boldsymbol{\omega}}} = \frac{\boldsymbol{\omega}^H \boldsymbol{R}_s \boldsymbol{\omega}}{\boldsymbol{\omega}^H \boldsymbol{R}_{c+n} \boldsymbol{\omega}} \frac{\sigma_0^2}{\sigma_s^2 NK} \tag{43}$$

where $\boldsymbol{R}_s$, $\boldsymbol{R}_{c+n}$ and $\boldsymbol{R}_n$ stand for the signal covariance matrix, clutter-plus-noise covariance matrix and noise covariance matrix, respectively. $\boldsymbol{\omega}$ is the space-time adaptive weight vector. σ_0^2 and σ_s^2 represent the noise and signal power, respectively.

Fig. 8(a) and Fig. 8(b) demonstrate the clutter spectra estimated by all slant range bins in the traditional PA radar and by the proposed method in the proposed PA-FDA dual-mode radar. In addition, an ideal clutter spectrum corresponding to PA is presented as a benchmark in Fig. 8(c). It is observed from Fig. 8(b) that the clutter spectra of near-range and far-range regions are separated similar to ideal clutter spectrum. The focused result of clutter spectrum is better compared to the PA in Fig. 8(a).

Fig. 9 depicts the SCNR loss of different methods, including the traditional STAP method in traditional PA with and without the DW compensation, and the proposed method in the PA-FDA dual-mode radar with and without noise reduction. Moreover, the ideal curves are also presented as a benchmark. It is observed that the SCNR loss performance of traditional PA in range-ambiguous clutter scenario

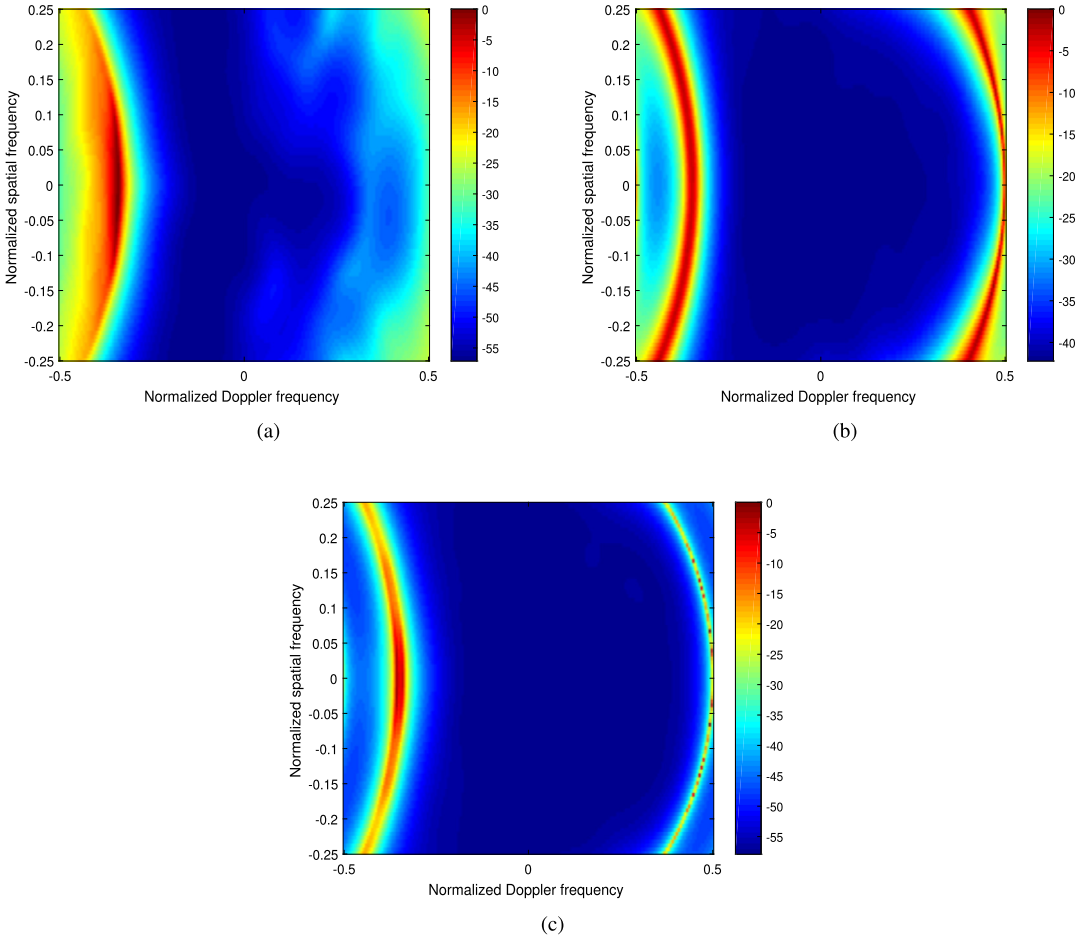

Fig. 8. Clutter spectrum distribution (a) Traditional PA radar (b) The proposed PA-FDA dual-mode radar (c) Ideal case.

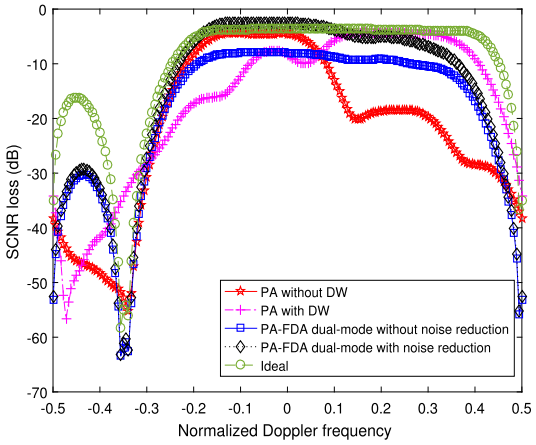

Fig. 9. SCNR loss versus normalized Doppler frequency.

is terrible since the range ambiguity and dependence cause a spread of the clutter spectrum. In the proposed PA-FDA dual-mode radar, the performance of range-ambiguous clutter suppression is superior to the conventional single PA radars. Moreover, it is seen that the performance of the SCNR loss is improved by using the proposed noise reduction method.

4.3. Analysis of detection performance in PA-FDA radar

In this section, the target detection performance of the proposed PA-FDA dual mode-radar is discussed in range-ambiguous clutter scenario. In particular, the number of transmitting elements of the single-mode radar is equal to the total number of transmitting elements of the proposed dual-mode radar for a fair comparison.

Fig. 10 shows the target SCNR output of the traditional single mode PA radar, single mode FDA radar and the proposed PA-FDA dual-mode radar, respectively. In this simulation, the input SNR, position and target velocity are set as 0 dB, 0° and 35 m/s, respectively. It is

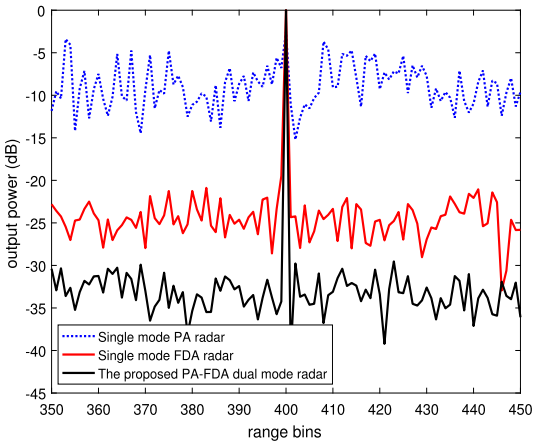

Fig. 10. Target SCNR output of different mode radar.

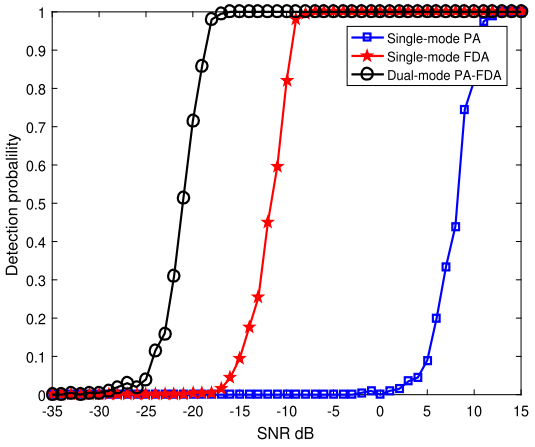

Fig. 11. Detection probability performance of different mode radar.

observed that, for the traditional single mode PA radar, the target SCNR output performance is so terrible since the Doppler frequency of the target is buried in the Doppler region occupied by the expanded clutter spectrum. Moreover, we can also see that the target can be detected by the single-mode FDA radar, while target SCNR output is reduced by about 10 dB compared with the proposed PA-FDA dual-mode radar. The reason is that FDA cannot form a high beampattern gain similar to PA. The target SCNR output of the proposed PA-FDA dual-mode radar is superior to the traditional single mode PA radar and single mode FDA radar in range-ambiguous clutter scenario.

To further verify the detection performance of the proposed PA-FDA dual-mode radar, Fig. 11 compares the detection probability performance of the above three radars with respect to the input SNR of the target, where false probability is set as 10^{-5}. It is observed that the detection probability of the proposed PA-FDA dual-mode radar is superior to the traditional single mode PA radar and single mode FDA radar. Notably, under the background of range-ambiguous clutters, the proposed dual-mode radar has a 25 dB performance improvement in moving target detection compared with the traditional PA radar. In conclusion, under the background of range-ambiguous clutters, the target detection performance of the proposed PA-FDA dual-mode radar is better than that of the traditional single mode PA radar and the single mode FDA radar. Therefore, the PA-FDA dual mode radar offers tremendous potential for tracking targets.

5. Conclusion

In this paper, a PA-FDA dual-mode STAP radar is established in signal-level fusion mode. A range ambiguous clutter suppression scheme for PA-FDA dual mode radar is presented. In the proposed method, the CCM of PA part is represented by using linear combination of distinguishable CCMs corresponding to different range regions in the FDA part. A noise power reduction method is devised to enhance the CCM estimation accuracy. The enhanced CCM is applied in PA counterpart, which maximizes the high beampattern gain of PA and range ambiguity resolvability of FDA. Simulation examples show that the PA-FDA dual-mode radar has a 25 dB SCNR improvement compared with the traditional PA radar. Area for future consideration should include approaches to overcome the limit of non-zero cross-correlation energy caused by imperfect orthogonal waveforms.

CRediT authorship contribution statement

Zhixin Liu: Conceptualization, Formal analysis, Methodology, Writing – original draft. **Shengqi Zhu:** Supervision, Writing – review & editing. **Jingwei Xu:** Formal analysis, Writing – review & editing. **Xiongpeng He:** Writing – review & editing. **Qi Liu:** Writing – review & editing.

Declaration of competing interest

The authors declare that they have no known competing financial interests or personal relationships that could have appeared to influence the work reported in this paper.

Data availability

The authors do not have permission to share data.

References

[1] W.L. Melvin, A STAP overview, IEEE Aerosp. Electron. Syst. Mag. 19 (1) (Jan. 2004) 19–35.
[2] A. Dallinger, B. Bickert, Airborne moving target indication of ground and maritime targets with smartRadar, in: 2014 International Radar Conference, 2014, pp. 1–5.
[3] J.R. Guerci, Space-Time Adaptive Processing for Radar, Artech House, Norwood, MA, USA, 2003.
[4] T.F. Ayoub, A.M. Haimovich, M.L. Pugh, Reduced-rank STAP for high PRF radar, IEEE Trans. Aerosp. Electron. Syst. 35 (3) (July 1999) 953–962.
[5] O. Kreyenkamp, R. Klemm, Doppler compensation in forward-looking STAP radar, IEE Proc. Radar Sonar Navig. 148 (5) (2001) 253–258.
[6] R. Klemm, Adaptive airborne MTI: comparison of sideways and forward looking radar, in: Proceedings International Radar Conference, 1995, pp. 614–618.
[7] S.D. Hayward, Adaptive beamforming for rapidly moving arrays, in: Proceedings of International Radar Conference, 1996, pp. 480–483.
[8] B. Himed, Y. Zhang, A. Hajjari, STAP for angle-Doppler compensation for bistatic airborne radars, in: Proceedings of the 2002 IEEE Radar Conference, Long Beach, CA, USA, May. 2002, pp. 311–317.
[9] P. Ries, F.D. Lapierre, J.G. Verly, Geometry-induced range dependence compensation for bistatic STAP with conformal arrays, IEEE Trans. Aerosp. Electron. Syst. 47 (1) (Jan. 2011) 275–294.
[10] V. Varadarajan, J.L. Krolik, Joint space-time interpolation for distorted linear and bistatic array geometries, IEEE Trans. Signal Process. 54 (3) (Mar. 2006) 848–860.
[11] D. Cristallini, W. Burger, A robust direct data domain approach for STAP, IEEE Trans. Signal Process. 60 (3) (March. 2012) 1283–1294.
[12] W. Choi, T.K. Sarkar, Minimum norm property for the sum of the adaptive weights for a direct data domain least squares algorithm, IEEE Trans. Antennas Propag. 54 (3) (March 2006) 1045–1050.
[13] W. Chen, W. Xie, Y. Wang, Short-range clutter suppression for airborne radar using sparse recovery and orthogonal projection, IEEE Geosci. Remote Sens. Lett. 19 (2022) 1–5.
[14] T.B. Hale, M.A. Temple, M.C. Wicks, Clutter suppression using elevation interferometry fused with space-time adaptive processing, Electron. Lett. 37 (12) (Jun. 2001) 793–794.
[15] X. Meng, T. Wang, J. Wu, Z. Bao, Short-range clutter suppression for airborne radar by utilizing prefiltering in elevation, IEEE Geosci. Remote Sens. Lett. 6 (2) (Apr. 2009) 268–272.
[16] T.B. Hale, M.A. Temple, J.F. Raquet, M.E. Oxley, M.C. Wicks, Localized three-dimensional adaptive spatial-temporal processing for airborne radar, IET Radar Sonar Navig. 150 (1) (Feb. 2003) 18–22.
[17] K. Duan, H. Xu, H. Yuan, H. Xie, Y. Wang, Reduced-DOF three-dimensional STAP via subarray synthesis for nonsidelooking planar array airborne radar, IEEE Trans. Aerosp. Electron. Syst. 56 (4) (Aug. 2020) 3311–3325.
[18] P. Antonik, M.C. Wicks, H.D. Griffiths, C.J. Baker, Range dependent beamforming using element level waveform diversity, in: Proceedings of the 2006 International Waveform Diversity and Design Conference, Las Vegas, NV, USA, Jan. 2006, pp. 140–144.
[19] W. Wang, Subarray-based frequency diverse array radar for target range-angle estimation, IEEE Trans. Aerosp. Electron. Syst. 50 (4) (October. 2014) 3057–3067.
[20] P. Antonik, M.C. Wicks, H.D. Griffiths, C.J. Baker, Frequency diverse array radars, in: Proceedings of the 2006 IEEE Conference on Radar, Verona, NY, USA, Apr. 2006, pp. 215–217.
[21] P. Baizert, T.B. Hale, M.A. Temple, M.C. Wicks, Forward-looking radar GMTI benefits using a linear frequency diverse array, Electron. Lett. 42 (22) (October. 2006) 1311–1312.
[22] J. Xu, G. Liao, S. Zhu, L. Huang, H.C. So, Joint range and angle estimation using MIMO radar with frequency diverse array, IEEE Trans. Signal Process. 63 (13) (July. 2015) 3396–3410.
[23] L. Lan, M. Rosamilia, A. Aubry, A. Demaio, G. Liao, Single-snapshot angle and incremental range estimation for FDA-MIMO radar, IEEE Trans. Aerosp. Electron. Syst., to be published, https://doi.org/10.1109/TAES.2021.3083591.
[24] J. Xu, G. Liao, S. Zhu, H.C. So, Deceptive jamming suppression with frequency diverse MIMO radar, Signal Process. 113 (Aug. 2015) 9–17.
[25] L. Lan, G. Liao, J. Xu, Y. Zhang, F. Fioranelli, Suppression approach to main-beam deceptive jamming in FDA-MIMO radar using nonhomogeneous sample detection, IEEE Access 6 (June. 2018) 34582–34597.
[26] J. Xu, G. Liao, Y. Zhang, H. Ji, L. Huang, An adaptive range-angle-Doppler processing approach for FDA-MIMO radar using three-dimensional localization, IEEE J. Sel. Top. Signal Process. 11 (2) (March 2017) 309–320.
[27] C. Wen, C. Ma, J. Peng, et al., Bistatic FDA-MIMO radar space-time adaptive processing, Signal Process. 163 (1) (May. 2019) 201–212.
[28] C. Wang, J. Xu, G. Liao, X. Xu, Y. Zhang, A range ambiguity resolution approach for high-resolution and wide-swath SAR imaging using frequency diverse array, IEEE J. Sel. Top. Signal Process. 11 (2) (March 2017) 336–346.
[29] J. Xu, S. Zhu, G. Liao, Range ambiguous clutter suppression for airborne FDA-STAP radar, IEEE J. Sel. Top. Signal Process. 9 (8) (Dec. 2015) 1620–1631.
[30] J. Xu, G. Liao, H.C. So, Space-time adaptive processing with vertical frequency diverse array for range-ambiguous clutter suppression, IEEE Trans. Geosci. Remote Sens. 54 (9) (Sep. 2016) 5352–5364.
[31] Y. Wang, S. Zhu, Range ambiguous clutter suppression for FDA-MIMO forward looking airborne radar based on main lobe correction, IEEE Trans. Veh. Technol. 70 (3) (March 2021) 2032–2046.
[32] R.H. Gui, W.Q. Wang, A. Farina, et al., FDA radar with Doppler-spreading consideration: main-lobe clutter suppression for blind-Doppler target detection, Signal Process. 179 (9) (Feb. 2021) 107773.
[33] C. Wen, M. Tao, J. Peng, et al., Clutter suppression for airborne FDA-MIMO radar using multi-waveform adaptive processing and auxiliary channel STAP, Signal Process. 154 (1) (Jan 2019) 280–293.
[34] C. Wen, Y. Huang, J. Peng, J. Wu, G. Zheng, Y. Zhang, Slow-time FDA-MIMO technique with application to STAP radar, IEEE Trans. Aerosp. Electron. Syst. 58 (1) (Feb. 2022) 74–95.
[35] W. Chen, W. Xie, Y. Wang, Range-dependent ambiguous cutter suppression for airborne SSF-STAP radar, IEEE Trans. Aerosp. Electron. Syst. 58 (2) (April 2022) 855–867.
[36] C. Gao, K.C. Teh, A. Liu, Orthogonal frequency diversity waveform with range-Doppler optimization for MIMO radar, IEEE Signal Process. Lett. 21 (10) (Oct. 2014) 1201–1205.
[37] H. He, P. Stoica, J. Li, Designing unimodular sequence sets with good correlations—including an application to MIMO radar, IEEE Trans. Signal Process. 57 (11) (Nov. 2009) 4391–4405.
[38] K. Wang, G. Liao, J. Xu, Y. Zhang, L. Huang, Clutter rank analysis in airborne FDA-MIMO radar with range ambiguity, IEEE Trans. Aerosp. Electron. Syst. 58 (2) (April 2022) 1416–1430.
[39] L. Hai, et al., Estimation of clutter degrees of freedom in airborne forward-looking radar via random matrix theory and minimum description length criteria, J. Electron. Inf. Technol. 38 (12) (2016) 3224–3229.
[40] C.Y. Chen, P.P. Vaidyanathan, MIMO radar space-time adaptive processing using prolate spheroidal wave functions, IEEE Trans. Signal Process. 56 (2) (2008) 623–635.

Zhixin Liu was born in Shandong, China. He received the B.S. degree in electronic engineering from Shandong Jiaotong University in 2017, and the M.S. degree in Electronics and Communication from Civil Aviation University of China in 2020. He is currently pursuing the Ph.D. degree in signal and information processing, in the National Key Laboratory of Radar Signal Processing, Xidian University, Xi'an, China. His research interests include waveform diverse array radar, space-time adaptive processing and multiple-input multiple-output radar.

Shengqi Zhu received the B.S. and Ph.D. degrees in electrical engineering from Xidian University, Xi'an, China, in 2005 and 2010, respectively. He is currently a Professor with Xidian University. His research interests include wave diversity radars (especially on frequency diverse array, time diverse array, and element-pulse coding array radars), adaptive signal processing, SAR ground moving target indication, and sparse signal processing. He is a member of the Young Talent of National Ten-Thousands Talents Program and the Outstanding Young Person in National Defense.

Jingwei Xu was born in Shandong, China. He received the B.S. degree in electronic engineering and the Ph.D. degree in signal and information processing from Xidian University, Xi'an, China, in 2010 and 2015, respectively. He is currently an Associate Professor with the School of Electronic Engineering, Xidian University. From 2015 to 2017, he was a Lecturer with the National Laboratory of Radar Signal Processing, Xidian University. From 2017 to 2019, he was a Postdoctoral Fellow under "Hong Kong Scholar Program" with the City University of Hong Kong. His research interests include radar system modeling, multi-sensor array signal processing, space–time adaptive processing, multiple-input multiple-output radar, and waveform diverse array radar. Dr. Xu was the recipient of the prize for an excellent Ph.D. degree dissertation from the Chinese Institute of Electronics in 2017. He won the Young Outstanding Talents of Shaanxi Province in 2020.

Xiongpeng He was born in Shaanxi, China, in 1992. He received the B.S. degree in electronic engineering and the Ph.D. degree in signal and information processing from Xidian University, Xi'an, China, in 2015 and 2020, respectively. He has been a Tenure-Track Associate Professor with the National Laboratory of Radar Signal Processing, Xidian University, since November 2020. His research interests include waveform diversity array (WDA), synthetic aperture radar (SAR), ground moving target indication (GMTI), and space–time adaptive processing (STAP)

Qi Liu received the bachelor's and master's degrees from Harbin Engineering University, Harbin, China, in 2013 and 2016, respectively, and the Ph.D. degree in electrical engineering from the City University of Hong Kong, Hong Kong, China, in 2019. He is currently a Professor with the School of Future Technology with the South China University of Technology. From 2018 to 2019, he was a Visiting Scholar with the University of California at Davis, Davis, CA, USA. From 2019 to 2022, he worked as a Research Fellow with the Department of Electrical and Computer Engineering, National University of Singapore, Singapore. His research interests include machine learning, optimization methods, and neuromorphic computing with applications to image/video/speech signal processing. He has been an Associate Editor of the IEEE SYSTEMS JOURNAL since 2022, and Digital Signal Processing since 2022. He was also a Guest Editor for the IET Signal Processing, International Journal of Antennas and Propagation, and Wireless Communications and Mobile Computing.